VTT Technical Research Centre of Finland

State of health estimation of cycle aged large format lithium-ion cells based on partial charging

Jenu, Samppa; Hentunen, Ari; Haavisto, Jari; Pihlatie, Mikko

Published in:
Journal of Energy Storage

DOI:
10.1016/j.est.2021.103855

Published: 01/02/2022

Document Version
Publisher's final version

Journal of Energy Storage 46 (2022) 103855

Contents lists available at ScienceDirect

Journal of Energy Storage

journal homepage: www.elsevier.com/locate/est

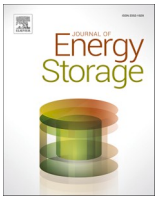

Research Papers

State of health estimation of cycle aged large format lithium-ion cells based on partial charging

Samppa Jenu [a,*], Ari Hentunen [a], Jari Haavisto [a], Mikko Pihlatie [a]

[a] VTT Technical Research Centre of Finland Ltd., P.O. Box 1000, FI-02044 VTT, Finland

ARTICLE INFO

Keywords:
Li-ion battery
Cycle ageing
Capacity fade
State of health
Incremental capacity analysis
Integrated voltage

ABSTRACT

Incremental capacity analysis (ICA) is a widely used method for assessing Li-ion battery state of health (SOH). The ICA method is typically applied to low C-rate charging or discharging, which is seldom feasible in online SOH estimation in real applications. In this paper the applicability of the ICA method to higher C-rates is investigated with C/3, 1C and 2C charging data from cycle aged large format commercial $LiFePO_4$/graphite cells, $LiNiMnCoO_2$/graphite cells, and cells with Li_2TiO_3 anode. Alongside the ICA method, a less studied integrated voltage (IV) method is investigated with the same data set. The results show that both the ICA method and the IV method can be used for battery SOH estimation utilizing partial charging data. The results for the ICA method indicate an accuracy of 0.9–2.1% (RMSE) with C/3 charging for all studied cells, and corresponding accuracy also for some of the cell types studied with 1C and 2C charging currents. The accuracy of the IV method does not suffer from increasing charging current as heavily as the accuracy of the ICA method, and the SOH estimation error remains below 2.0% (RMSE) with all studied cell types up to 2C charging.

1. Introduction

Lithium-ion batteries have become a key energy storage solution for the electrification of transport, from electric passenger cars to heavy-duty electric commercial vehicles, as well as for stationary energy storage systems. The main driver for using Li-ion batteries in transportation and stationary applications is to reduce carbon dioxide emissions. The environmental impact of Li-ion batteries significantly depends on the battery life, which is limited by battery degradation. The degradation occurs during battery operation and idle time, and its rate is affected by the operating schemes and environmental conditions of the battery [1,2]. Exposing the battery to more demanding use, such as frequent charging and discharging with high current rates or operation at suboptimal temperatures, accelerates the degradation. The degradation of lithium-ion batteries is a complex combination of chemical, physical and mechanical processes, which lead to decrease in battery capacity and increase in battery impedance [1,3]. The broad array of degradation mechanisms can be clustered into three main degradation modes: loss of lithium inventory, loss of active anode material and loss of active cathode material [4].

The degradation rate and lifetime of Li-ion batteries in different operating conditions has been examined and reported in various studies in the literature. Several cycle ageing studies have been reported for small (1.1–3 Ah) cylindrical lithium iron phosphate (LFP) cells [5–10], but only one study for large LFP pouch cells was found [11]. Additionally, in [12], Lewerenz et al. have examined the cycle ageing of 8 Ah cylindrical LFP cells in different operating conditions. Comprehensive cycle ageing studies have been reported also for cylindrical 18650 format lithium nickel manganese cobalt oxide (NMC) cells [13–16]. For these small cylindrical cells, the utilized C-rates are typically 1C or lower. In [15] and [16] also 2C discharge has been used with some 18650 format NMC cells. In addition, many cycle ageing studies for larger NMC cells can be found from the literature [17–24]. Several studies include also cells cycled with C-rates up to 2C or 3C [19–21,23,24]. In [22], Gao et al. have cycled commercial 8 Ah NMC pouch cells with a C-rate as high as 6C for both charging and discharging. A considerably less studied and reported Li-ion battery type is cells with lithium titanate (LTO) anodes. In [25], Takami et al. present cycle ageing results from prototype LTO cells. Han et al. study the cycle ageing of three commercial LTO cells in [26]. In more recent studies [27–29], the cycle life of commercial 11–13 Ah LTO cells has been examined with different cycling conditions. In [27] and [28] the cells have been cycled with up to 3C, whereas in [29] the cells have been cycled with as high as 5C and 10C.

Cycle ageing tests are often performed on small cylindrical cells and

* Corresponding author.
E-mail address: samppa.jenu@vtt.fi (S. Jenu).

https://doi.org/10.1016/j.est.2021.103855
Received 17 February 2021; Received in revised form 13 August 2021; Accepted 14 December 2021
Available online 22 December 2021

Acronyms

BMS	battery management system
CC	constant-current
CV	constant-voltage
DOD	depth of discharge
DVA	differential voltage analysis
ECM	equivalent circuit model
EFC	equivalent full cycle
EIS	electrochemical impedance spectroscopy
IC	incremental capacity
ICA	incremental capacity analysis
IV	integrated voltage
LCO	lithium cobalt oxide
LFP	lithium iron phosphate
LTO	lithium titanate
MA	moving average
NMC	lithium nickel manganese cobalt oxide
RMSE	root mean square error
SOC	state of charge
SOH	state of health

thus there is a need for experimental results with large format pouch cells. In this study we consider 20 Ah or larger cells as large format cells to distinguish pouch or prismatic cells used in electric vehicles or industrial applications from small cylindrical or coin cells commonly used in consumer applications. Limited number of studies exists where large format Li-ion cells are tested with high charge rates, especially for LFP cells. The work presented in this paper contributes to the existing literature by providing results and analysis from such experiments.

The degree of battery degradation is measured with battery state of health (SOH). SOH describes the present condition of the battery compared to fresh battery. Battery SOH can be determined according to several factors of which battery energy capability and power capability are the most common [30]. These are indicated by battery capacity fade and impedance increase, respectively. In this study, SOH is determined based on battery capacity.

Numerous methods for SOH estimation of Li-ion batteries have been introduced in the literature [30–33]. The SOH estimation methods can be divided into two groups: experimental methods and model-based estimation methods [30]. The experimental methods can be based on direct measurements like the Coulomb counting based methods [34], estimation of internal resistance from current pulses [35] or measuring the impedance of the battery with electrochemical impedance spectroscopy (EIS) [36]. In addition to the direct experimental methods, several indirect analysis methods such as incremental capacity analysis (ICA) [26,37,46,38–45] or differential voltage analysis (DVA) [26,38,40] have been commonly used for Li-ion battery degradation analysis and SOH estimation. The challenge in utilizing these experimental methods in real applications is that they rely on specific experimental measurements, which may not be feasible during the normal operation of the battery system.

To achieve robust real-time battery health monitoring, various model-based methods have been developed. The model-based SOH estimation methods commonly rely on an equivalent circuit model (ECM) of the examined battery. A frequently used approach is to utilize Kalman filters to update the ECM parameters online and estimate the battery SOH [47]. In addition to ECM models, also other types of models including electrochemical models, empirical lifecycle models, mathematical models or machine learning methods, such as neural networks or support vector machine, have been developed for Li-ion battery SOH estimation [32]. Advanced battery models can estimate the state of the battery accurately, but on the other hand, they typically require high computational power or may require extensive work to parametrize the battery model.

Incremental capacity analysis has been applied for LFP [37–39,41,44–46] and NMC [40,42,43] cells as well as for LTO [26,38] cells. The degradation mechanisms of LFP cells have been analysed in detail studying the evolution of incremental capacity (IC) curves from charging or discharging with low C-rates (e.g. C/10 or C/25) [37,44,45]. ICA with low C-rate data can provide accurate results, but such a low C-rate data is typically not available during the use of the battery in real applications. The challenge with higher C-rates is that the smaller peaks in the IC curves often shrink to unnoticeable when the current is increased. Another challenge in online ICA is the noise in the measurements, which makes it difficult to form a clear IC curve. Different filtering methods such as Butterworth filter [39], Gaussian filter [42], Kalman filter [43] or support vector regression [41] have been utilized to obtain a smooth IC curve. Online SOH estimation with ICA has been presented for LFP cells [39,41,46] and NMC cells [40,42,43], but no study specifically on online ICA for LTO cells was found. In the referenced literature, online ICA was performed with C-rates up to 1C. In this study, ICA is applied to constant current phase data from standard CC—CV charging of LFP, NMC and LTO cells with C/3, 1C and 2C charging rates to examine the feasibility of the ICA method in real applications.

Stroe et al. [48] and Schaltz et al. [49] have introduced a SOH estimation method which they call partial charging method. The partial charging method focuses on the measurement of battery charging capacity for a reduced voltage interval. They have tested the method with NMC cells at different stages of ageing and have detected a clear relationship between the partial charging capacity and full discharge capacity. Another SOH estimation method based on charging curves is the integrated voltage (IV) method introduced by Zhou et al. [50]. Integrated voltage method utilizes battery voltage data during constant current charging to estimate the capacity fade of the battery. In [50], Zhou et al. demonstrated the IV method with C/2 charging of LCO cells. Like the ICA method, the IV method is applied in this study to charging data from LFP, NMC and LTO cells with C/3, 1C and 2C charging rates. In addition, the applicability of the IV method to partial charging data is investigated utilizing different voltage ranges.

The remainder of the paper is structured as follows: Firstly, the cycle ageing experiments performed on LFP, NMC and LTO cells are described in Section 2. Secondly, the SOH estimation methods addressed in this study are explained in Section 3. In Section 4, the results from the cycle ageing experiments and the SOH estimation methods are presented and discussed. Finally, Section 5 summarizes the main conclusions.

2. Experimental

The experimental work was performed on twelve commercial A123 20 Ah $LiFePO_4$/graphite pouch cells, three commercial Kokam 40 Ah $LiNiMnCoO_2$/graphite pouch cells and three commercial Kokam 65 Ah pouch cells with Li_2TiO_3 anode. The cathode material of Kokam LTO cells is not specified by the manufacturer. The basic parameters of the

Table 1.
Basic parameters of examined batteries.

	A123 LFP	Kokam NMC	Kokam LTO
Battery type	LFP / C	NMC / C	? / LTO
Nominal capacity	20 Ah	40 Ah	65 Ah
Nominal voltage	3.3 V	3.7 V	2.2 V
Charge cut-off voltage	3.6 V	4.2 V	2.7 V
Discharge cut-off voltage	2.0 V	2.7 V	1.5 V
Maximum charge current	60 A (3C)	120 A (3C)	260 A (4C)
Maximum discharge current	60 A (3C)	320 A (8C)	260 A (4C)
C/3 discharge capacity [1]	19.8 Ah	43.0 Ah	65.3 Ah
Specific energy [1]	126 Wh/kg	164 Wh/kg	76.9 Wh/kg

[1] Experimentally determined average value for the lot.

examined Li-ion batteries are shown in Table 1.

The experimental tests consisted of initial characterization tests, cycle ageing tests and reference performance tests between the cycle ageing tests. The initial characterization test regime consisted of a pre-conditioning test, a capacity test, a dynamic test, a pulse test, and an electrochemical impedance spectroscopy (EIS). In the pre-conditioning test, three consecutive C/3 charge-discharge cycles were performed within the cut-off voltage limits defined by the manufacturer. The capacity test measured both the charge and discharge capacities of the cells with different C-rates, including C/3, 1C, 2C, and maximum allowed C-rate for a charge-discharge cycle, which is 3C for LFP and NMC cells, and 4C for LTO cells. The dynamic test was done according to the IEC 61982–2 to evaluate the dynamic performance of the cells, and the pulse test comprised equal charge and discharge pulses of 10 second duration with various C-rates. The EIS was done in a galvanostatic mode at different state of charge (SOC) levels.

After the cells were characterized, they entered the cycle ageing tests. The cells were cycled with different SOC ranges and different charge and discharge rates. The cycle ageing test matrix is shown in Table 2. The LFP cells were cycled with symmetric (2.5C charge/2.5C discharge) and asymmetric (2.5C charge/1C discharge and 1C charge/2.5C discharge) high currents and with different SOC windows. The SOC windows were 0–100%, 0–80%, and 20–100%. In the 0–100% SOC window, discharge was done until lower voltage was reached and a constant current-constant voltage (CC—CV) protocol was applied in charging. In the 0–80% SOC window, a minimum voltage limit was used to end discharge and Ah-counting was used to end the charge at 80%. In the 20–100% SOC window, the cell was charged with the CC—CV protocol and then discharged 80% with Ah-counting. In the cycle ageing tests the NMC and LTO cells were charged with maximum continuous charging rate specified by the manufacturer and discharged with 1C discharge rate. The maximum continuous charging rate for the tested NMC cells is 3C (120 A) and for the LTO cells 4C (260 A). The SOC window for cycling was 0–100%. CC—CV protocol was applied in charging and minimum voltage limit was used to end discharge. For all tested cells, a 10-minute rest period after both charge and discharge was allowed to stabilize temperature.

The reference performance test was done every 250 cycles for LFP cells and every 500 cycles for NMC and LTO cells (counted in actual charge-discharge cycles) to evaluate the state of health (SOH) of the cells. The reference performance test included the capacity test and the pulse test as specified above. During the cycle ageing tests, the cells were positioned on fume hood shelves and the ambient temperature was kept at 24 ± 1 °C. The LFP cells were placed between cooling elements and forced air cooling was used to minimize thermal cycling. The NMC and LTO cells were cycled without additional cooling. The ambient temperature in the fume cupboard and the temperature from the cell surface were monitored during all tests. The LFP cells were cycled with PEC SBT0550 battery testing equipment and their surface temperatures were measured with K-type thermocouples. The NMC and LTO cells were cycles with PEC ACT0550 battery testing equipment and their surface temperatures were measured with NTC thermistors. The ambient temperatures in all tests were measured with K-type thermocouples.

Table 2.
Cycle ageing test matrix.

Battery type	Charge rate (+)/ Discharge rate (-)	SOC range		
		0–100%	0–80%	20–100%
A123 LFP	+2.5C/−2.5C	2 cells	2 cells	2 cells
A123 LFP	+2.5C/−1C	1 cell	1 cell	1 cell
A123 LFP	+1C/−2.5C	1 cell	1 cell	1 cell
Kokam NMC	+3C/−1C	3 cells	–	–
Kokam LTO	+4C/−1C	3 cells	–	–

3. SOH estimation based on partial charging

Many SOH estimation methods presented in the literature utilize data from the discharge phase of the battery. However, constant discharge in controlled conditions is seldom available during the normal operation of the battery in real application. On the contrary, constant current-constant voltage (CC—CV) protocol is commonly used for charging Li-ion batteries in various applications. In this section, two SOH estimation methods that utilize partial charging data from the constant current phase are presented.

3.1. Incremental capacity analysis

Incremental capacity analysis (ICA) can be used to analyse the condition of the battery using data from charge or discharge phase. In ICA the charged or discharged capacity of the battery is differentiated with respect to the battery terminal voltage to obtain the incremental capacity (IC) curve:

$$IC = \frac{dQ}{dV}$$

where Q is the charged or discharged capacity and V is the terminal voltage of the battery. The charged or discharged capacity (Q) can be obtained utilizing the commonly used Coulomb counting method in which the current data is integrated over time to calculate the capacity charged to or discharged from the battery:

$$Q = \int_{t_1}^{t_2} I(t)dt$$

where t_1 and t_2 are the starting and ending times of the charge or discharge phase, and $I(t)$ is the current data.

In the IC curve, there are characteristic peaks depending on the battery chemistry. The peaks in the IC curves are related to lithium intercalation processes and phase transformations in the electrodes during charging or discharging of the battery [37,39]. Each peak has unique height, shape and position. Clear changes in IC curve peak height, area and position as a function of cell degradation are reported in the literature [26,37,38,40,45]. The changes in the IC curve reflect the changes in the behavior and electrochemical properties of the cell. The decrease of the peaks is linked to the loss of lithium inventory or loss of active material, whereas the shift of the peaks towards higher voltages is related to the increase of cell resistance [37,38,45]. Therefore, ICA is a suitable method to analyse the degradation mechanisms as well as monitor the SOH of the battery. ICA can be implemented for both charging and discharging data. As constant current charging or discharging data is required, analysing the charging data is typically more practical in real applications. In this study, the correlation between cell capacity fade and reduction in IC curve peak height and area was analysed.

As the IC curve is calculated by differentiating a measure-based quantity with respect to another measured quantity, even small fluctuation in the measured data easily causes large amount of noise to the obtained IC curve. Therefore, filtering the data is essential to obtain smooth and usable IC curves. In this study, the IC curve was smoothed with moving average filter and Gaussian filter using a similar approach to that presented by Li et al. in [42]. An example of the IC curve smoothed with moving average filter and Gaussian filter is presented in Fig. 1.

The height of the IC curve peak describes the charge transfer rate at the examined voltage level. The area of the peak, in turn, describes the amount of charge transferred within a certain voltage range. The amount of charge transferred within the voltage range can be calculated by either integrating the IC curve over the voltage range (peak area) or calculating the charged or discharged capacity from the current data during the corresponding time interval. The height of the peak is

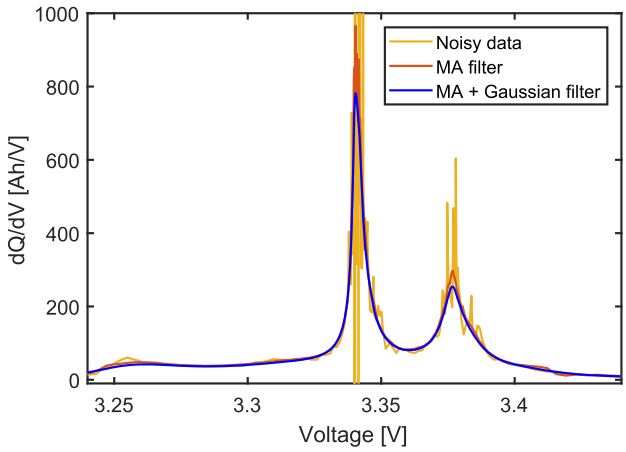

Fig. 1. IC curve smoothed with moving average (MA) filter and Gaussian filter. The data is from LFP cell C/3 charging.

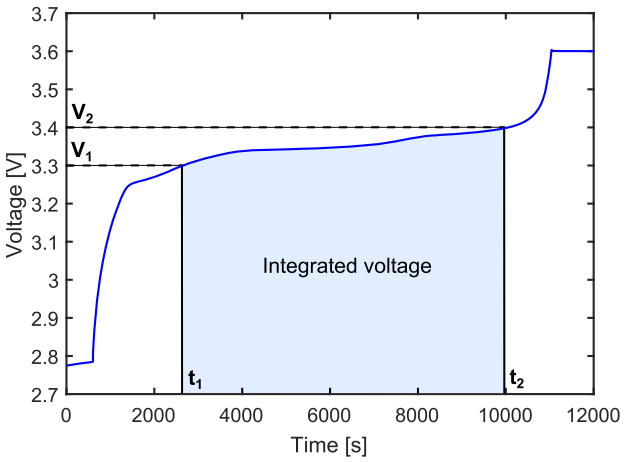

Fig. 2. Determination of the integrated voltage from LFP cell C/3 charging data.

straightforward to obtain from the filtered IC curve. On the other hand, for the area of the peak there is no exact definition. The voltage range for calculating the area of the peak can be defined based on a constant distance from the maximum of the peak or based on the shape of the peak.

In [43], Tang et al. use a voltage range with minimum and maximum at the same constant distance from the peak maximum and name the capacity change over that range as regional capacity. Tang et al. observe a linear relation between the regional capacity and the capacity-based SOH of the battery. Riviere et al. [46] estimate the SOH of LFP batteries by observing the change in the area of the second largest peak in the IC curve. In [46], the changes are examined by calculating the area under the IC curve in a constant voltage range starting from the maximum of the largest peak and covering the second largest peak.

In ICA, the SOH of the battery can be estimated by detecting changes in the height or area of a single peak in the IC curve. Therefore, the ICA method can be utilized even if only partial charging data is available. The sufficient voltage range, and the corresponding SOC range, depends on the observed Li-ion battery chemistry.

3.2. Integrated voltage method

Another method for battery SOH estimation applied in this study is the integrated voltage method introduced by Zhou et al. in [50]. In the integrated voltage method, the battery voltage during constant current charging is integrated over time in predefined voltage range ($V_1 \ldots V_2$) to obtain the integrated voltage:

$$IV = \int_{t_1}^{t_2} V(t)\, dt$$

where IV is the integrated voltage, t_1 is time at predefined minimum voltage V_1 and t_2 is time at predefined maximum voltage V_2 and $V(t)$ is the battery terminal voltage. The determination of the integrated voltage is presented in Fig. 2. The integrated voltage covers the whole area from t_1 to t_2 below the voltage curve and above 0 V, including the lower part that is not visible in the figure.

Changes in the obtained integrated voltage value (IV) correlate with the ageing of the cell. In [50], Zhou et al. observed a strong linear relation between the integrated voltage and the SOH of the studied LCO cells. They calculated the integrated voltage from C/2 charging between 3.85 V and 4.2 V, which corresponds to approximately 12–89% SOC for the LCO cells. In this study, the integrated voltage method was tested on LFP, NMC and LTO cells for C/3, 1C and 2C charging data and varying the voltage range. For different Li-ion chemistries, the shape of the voltage curve during charging is different and thus the voltage limits corresponding to certain SOC values are different. In general, the wider the voltage range the better the correlation between the integrated voltage and the SOH of the battery as long as the charging is performed within the constant current region.

The integrated voltage method is simple to implement and does not require heavy computations, and therefore it is feasible for battery management systems (BMS) with limited computational power. In principle, the integrated voltage method is quite similar to the ICA method if the area of the IC curve peaks is studied in a certain voltage range, but the integrated voltage method is more straightforward to implement and the only required input is the battery voltage measurement during constant current charging phase. The voltage range for the analysis can be selected according to the charging data available, which makes the integrated voltage method suitable also for applications with partial charging.

4. Results and discussion

4.1. Cycle ageing results

The cycle ageing test results of all tested LFP, NMC and LTO cells are compiled in Table 3. The amount of cycles cycled is reported in actual charge-discharge cycles and in equivalent full cycles (EFC). The amount of EFCs was calculated by multiplying the amount of actual cycles with the cycle depth of the charge-discharge cycle. The SOH is calculated by comparing the current C/3 discharge capacity to the initial C/3 discharge capacity of a fresh cell. The cycle ageing tests of the LFP cells lasted in total 190–1020 days including the time required for reference performance tests. Some of the LFP cells have long testing times due to idle time between the tests. The tests with higher C-rates were finished in shorter calendar time. The cycle ageing tests of the NMC and LTO cells lasted in total 350–420 days. The test results for LFP, NMC and LTO cells are analysed in more detail in Sections 4.1.1, 4.1.2 and 4.1.3.

The surface temperatures of the cells were monitored during the cycling. For all tested LFP cells the average surface temperature was 24–25 °C, which was approximately 1 °C higher than the ambient temperature at the same time. The highest surface temperature was monitored at the end of the high C-rate charging or discharging. The maximum measured surface temperatures for all tested LFP cells were in the range of 25–28 °C. No significant difference was observed between the cells cycled with different C-rates or SOC windows. The cell temperatures at 90% SOH and 80% SOH were also compared, and there was no noticeable difference. The average surface temperatures during cycling for tested NMC and LTO cells were in the range of 28–32 °C, which was 4–7 °C higher than the ambient temperature at the same

Table 3
Cycle ageing test results for all tested LFP, NMC and LTO cells. The SOH value corresponds to the end of the cycling test, and the performed cycles are reported in actual cycles and equivalent full cycles (EFC). In addition, cycles (EFC) at 80% SOH are reported.

Cell	SOC range	Charge rate (+)/discharge rate (-)	SOH	Cycles	Cycles (EFC)	Total test duration (d)	Cycles at 80% SOH (EFC)
LFP1	0–100%	+2.5C/−2.5C	79.2%	1750	1750	260	1680
LFP2	0–100%	+2.5C/−2.5C	46.9%	1750	1750	190	1500
LFP3	0–100%	+1C/−2.5C	68.2%	3797	3797	630	3040
LFP4	0–100%	+2.5C/−1C	68.2%	3000	3000	730	2420
LFP5	0–80%	+2.5C/−2.5C	79.6%	2000	1600	250	1570
LFP6	0–80%	+2.5C/−2.5C	78.4%	2000	1600	250	1460
LFP7	0–80%	+1C/−2.5C	74.9%	5227	4182	740	3880
LFP8	0–80%	+2.5C/−1C	63.0%	4400	3520	670	3300
LFP9	20–100%	+2.5C/−2.5C	79.0%	2250	1800	240	1710
LFP10	20–100%	+2.5C/−2.5C	78.0%	2000	1600	220	1430
LFP11	20–100%	+1C/−2.5C	69.7%	4750	3800	1020	3340
LFP12	20–100%	+2.5C/−1C	72.4%	3000	2400	630	2090
NMC1	0–100%	+3C/−1C	78.2%	4500	4500	420	4300
NMC2	0–100%	+3C/−1C	52.7%	4500	4500	360	4040
NMC3	0–100%	+3C/−1C	49.5%	4860	4860	400	4510
LTO1	0–100%	+4C/−1C	70.8%	5500	5500	410	5120
LTO2	0–100%	+4C/−1C	71.8%	4500	4500	350	4220
LTO3	0–100%	+4C/−1C	77.2%	5500	5500	420	5340

time. Maximum surface temperatures were reached at the end of the charging, and for the NMC and LTO cells they were 39–41 °C and 38–42 °C, respectively. When comparing the maximum surface temperatures, it should be noted that the NMC and LTO cells did not have active cooling unlike the LFP cells. The results show that without proper cooling high C-rate charging or discharging heats the cells significantly, which may accelerate battery degradation.

4.1.1. LFP cells

The cycle ageing test results for tested LFP cells are presented in Fig. 3. The six cells tested with 2.5C charge/2.5C discharge cycle reached 80% of initial capacity between 1430 to 1710 equivalent full cycles (EFCs). One of the cells (LFP2) cycled with 100% depth of discharge (DOD) experienced a sudden death by losing 33.3% of its capacity during the last 250 cycles. A significant increase in the lifetime was observed with the six cells cycled with asymmetric cycles. The three cells tested with 1C charge/2.5C discharge cycle reached 80% of initial capacity between 3040 to 3880 EFCs. The manufacturer specifies the lifetime of the cell to be over 3000 before 80% of initial capacity is reached with 100% DOD and 1C charge/2C discharge cycle. Therefore, it can be said that the cells performed as promised because with 100% DOD 1C charge/2.5C discharge cycle the capacity was 80.4% from initial at 3000 cycles. The three cells tested with 2.5C charge/1C discharge reached 80% of initial capacity between 2090 to 3300 EFCs.

The results, presented in Fig. 3, show clearly that high charging and discharging currents close to the maximum currents defined by the manufacturer speed up the cell degradation. Lowering either the charging or the discharging current extended the cell lifetime significantly. High charging current seems to be more detrimental than high discharging current. Decreasing the charging rate from 2.5C to 1C approximately doubled the cycle life of the cell even though the discharging rate was kept at 2.5C. For some tested cells the narrower SOC window resulted in longer cycle life, but the effect was not observed for all the cells cycled at 0–80% SOC or 20–100% SOC. A similar phenomenon was observed for the average SOC. Cycling the cell at 0–80% SOC was observed to lead to decreased capacity fade compared to the cell cycled at 20–100% SOC, but a clear difference was observed only in combination with high charging current (LFP8 and LFP12). For the cells with high charging current and high discharging current there was no notable difference. Overall, for most of the LFP cells the capacity fade accelerated after 80% SOH.

4.1.2. NMC cells

The cycle ageing test results for tested NMC cells are presented in Fig. 4. Three NMC cells were tested with 3C charge/1C discharge cycle with 100% DOD. The cells reached 80% of initial capacity between 4040 to 4510 cycles. The cell manufacturer specifies the cycle life of the cells to be up to 5000 cycles with 1C charge/1C discharge and 80% DOD, which is in line with the results obtained with the performed more demanding cycling. The capacity fade of all three cells was linear during

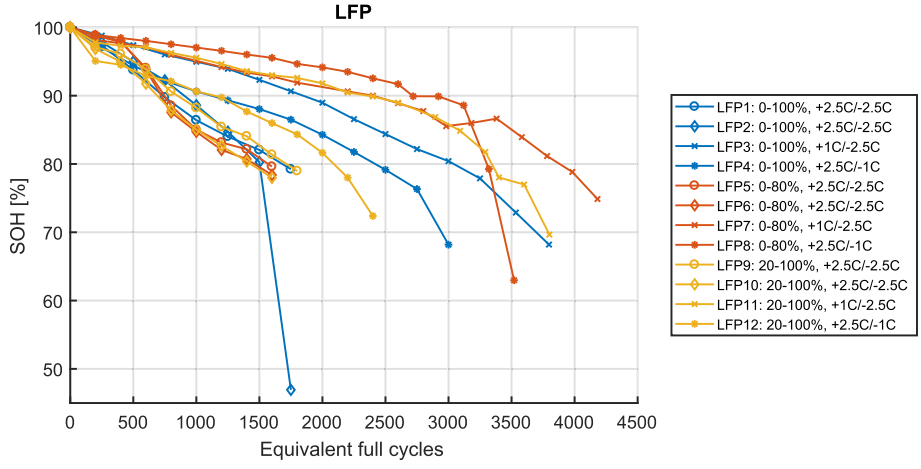

Fig. 3. Cycle ageing test results for LFP cells.

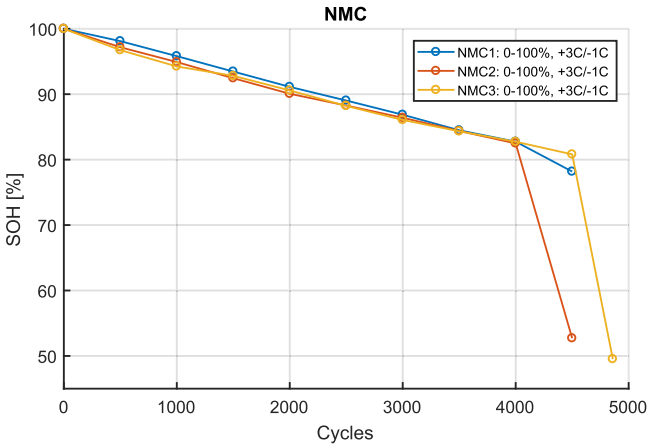

Fig. 4. Cycle ageing test results for NMC cells.

first 4000 cycles, after which one cell experienced a sudden death by losing 29.8% of its initial capacity during the last 500 cycles. The other two cells lasted a little longer before the accelerated capacity fade. For the NMC cells a so-called knee point, after which the degradation rate clearly increases, is very clear and is located approximately at 80% SOH.

4.1.3. LTO cells

The cycle ageing test results for tested LTO cells are presented in Fig. 5. Three LTO cells were tested with 4C charge/1C discharge cycle with 100% DOD. The capacity fade of the cells was quite uniform during the first 3500 cycles. At 500 cycles, a slight capacity increase compared to the initial capacity was detected, but after that the capacity fade was continuous and fairly linear. After 3500 cycles, the degradation rates of the cells diverged. The cells reached 80% of initial capacity between 4220 to 5340 cycles. The manufacturer reports a cycle life of over 10,000 cycles with 1C charge/1C discharge and over 5000 cycles with 4C charge/4C discharge, both with 100% DOD. Thus, the observed cycle life was somewhat shorter than would be expected based on the manufacturer's reports. For the LTO cells, the knee point is not as distinctive as for the NMC cells (Section 4.1.2), but an increase in the degradation rate can be observed around 85% SOH.

4.2. SOH estimation

4.2.1. Incremental capacity analysis

The C/3 charging data from the reference performance tests of the cycle-aged cells was analysed with incremental capacity analysis at different stages of ageing. The evolution of the IC curves as a result of battery ageing for studied LFP, NMC and LTO cells is presented in Fig. 6.

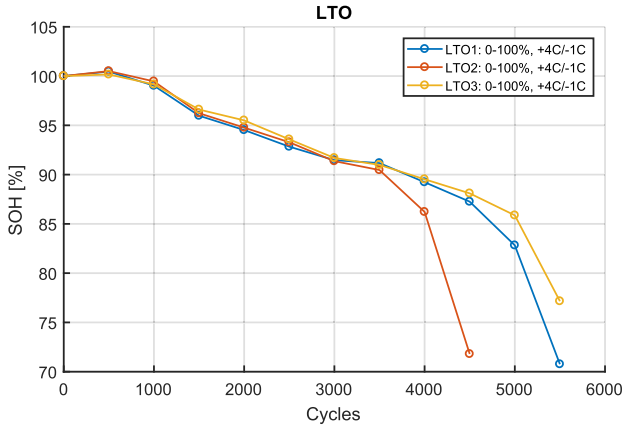

Fig. 5. Cycle ageing test results for LTO cells.

Each Li-ion chemistry has unique IC curve shape, but in all of them, there are characteristic peaks that decrease as the battery ages. The IC curve of the LFP cell (Fig. 6a) has two distinctive peaks: one around 3.34 V and another around 3.38 V. Up to five peaks have been reported in the literature when the LFP cell is charged with a really low C-rate [37,45]. However, in this case already the third peak around 3.25 V is almost unnoticeable when charged with C/3. Both the largest and the second largest peak decrease as a function of charge-discharge cycles, but the change in the location of the peaks is not significant. The correlation of the height and area of the two largest peaks with the available discharge capacity of the cell was studied and the best correlation was observed with the area of the second largest peak (around 3.38 V). The best method for determining the area of the second largest peak was found to be the method introduced by Riviere et al. [39], in which the area under the IC curve in a constant voltage range starting from the maximum of the largest peak and covering the second largest peak is calculated. For the studied LFP cells, a voltage range of 0.065 V was used. The correlation between the area of the second largest peak and the SOH of the cell is presented in Fig. 7. The SOH was calculated based on the discharge capacity of the battery. A second-degree polynomial curve was fit to the data to model the correlation. When the charging rate is increased, the second largest peak begins to merge with the largest peak. With 1C charging the second largest peak is almost undetectable, but the results obtained by calculating the area under the IC curve with the aforementioned method still correlate with the SOH of the cell, albeit with lower accuracy. The root mean square error (RMSE) of the fitted model is 2.12% for C/3 charging and 2.33% for 1C charging. With 2C charging the obtained data points scatter even more resulting in poor accuracy.

In the IC curve of the NMC cell (Fig. 6b), there are two clear peaks: the main peak around 3.7 V and a smaller side peak around 3.55 V. Both peaks decrease and shift clearly towards higher voltages as the cell ages. Similar IC curve shape has been detected for NMC cells in [42] and [40], especially for the largest peak. In [40], Berecibar et al. observe that the largest peak decrease and shift is mainly related to the loss of lithium inventory. The shift of the peaks towards higher voltages may also be due to increase in cell internal resistance. The height of the largest peak in the IC curve was observed to correlate with the available discharge capacity of the studied NMC cells. The correlation is good with the accuracy of 1.37% (RMSE) for C/3 charging and 1.60% (RMSE) for 1C charging, but with 2C charging the data points begin to disperse from the fitted model as can be seen in Fig. 7.

In the IC curve of the LTO cell (Fig. 6c), there is only one wide peak, which covers virtually the entire voltage range of the charging. The maximum of the peak is around 2.2 V, which corresponds to approximately 20% SOC. As the peak is so wide, calculating the area of the peak would require data from a full 0% to 100% SOC charge. If only partial charging data is available, which is often the case in practical applications, either the height of the peak or the area of the peak in certain voltage interval can be examined. For the studied LTO cells, a good correlation between the height of the peak and the available discharge capacity of the cell was observed. Additionally, a clear correlation between the area of the peak within various limited voltage intervals (e.g. voltage interval corresponding to 40–60% SOC) and the discharge capacity of the cell was observed. This relation can be exploited if the maximum of the IC curve peak is outside the voltage range of the partial charging data available. The correlation between the height of the IC curve peak and the SOH of the studied LTO cells is presented in Fig. 7. The results obtained from C/3 charging follow the fitted model with 0.85% (RMSE) accuracy. With 1C and 2C charging the data points are slightly more scattered, but still follow the fitted model with reasonable accuracy of 1.58% and 1.57% (RMSE).

The results presented in Fig. 7 show that in general increasing the charging current decreases the accuracy of the ICA method. The sensitivity of the ICA method to the utilized C-rate depends on the cell type. When the C-rate is increased, the characteristic peaks in the IC curve

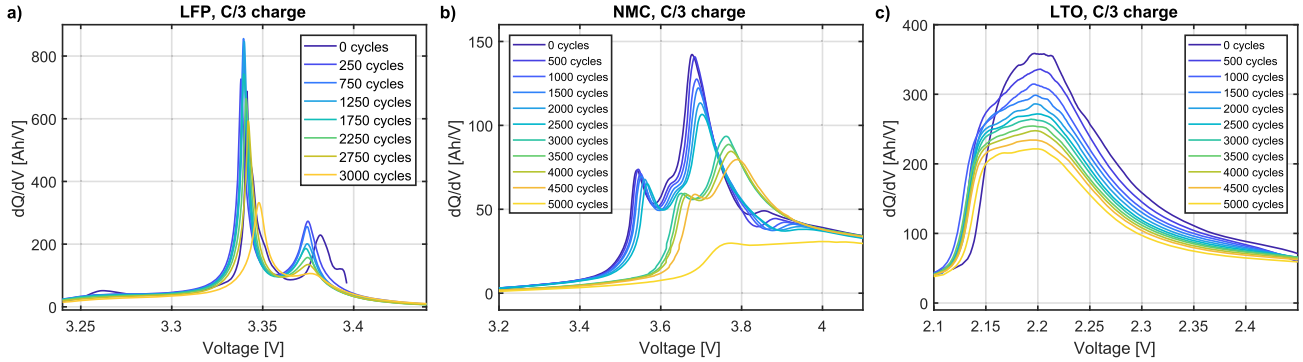

Fig. 6. Evolution of incremental capacity curve as a function of charge-discharge cycles for a) LFP cell, b) NMC cell, c) LTO cell.

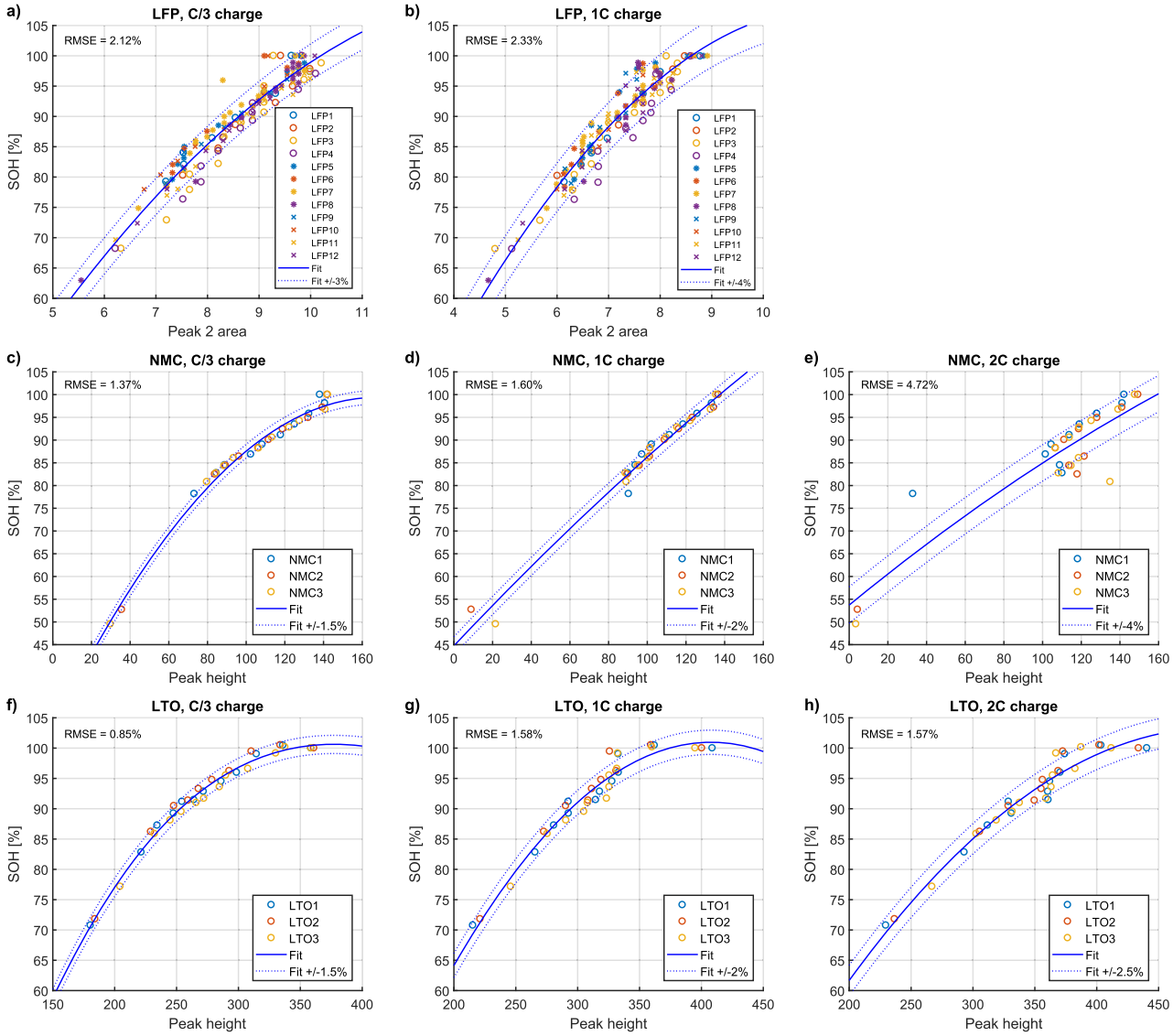

Fig. 7. The results of the incremental capacity analysis method for LFP cells (a-b), NMC cells (c-e) and LTO cells (f-h) with different C-rates. The root mean square error (RMSE) of the fitted model is marked on each figure.

gradually become less distinctive. LFP cells have significantly narrower characteristic peaks than NMC or LTO cells, and therefore the increase in C-rate is more strongly reflected in the decrease in the accuracy of the ICA method. The results for the studied LFP cells start to scatter already with 1C charging, whereas the results for the studied NMC cells with 1C and the studied LTO cells with 2C are still relatively accurate. In addition, it was observed that the utilized voltage (or SOC) range affects the accuracy of the results if SOH is estimated based on the area of the IC curve peak. If the observed IC curve peak is only partially covered by the available voltage range, the accuracy of the method decreases. If SOH is

estimated based on the height of the IC curve peak, the extent of the voltage range available does not affect the accuracy of the method as long as the maximum of the peak is within the voltage range.

4.2.2. Integrated voltage method

Integrated voltage method was applied to C/3, 1C and 2C charging data from all the examined cells at different stages of ageing. The correlation between the integrated voltage and the SOH of the battery was studied by fitting a polynomial curve (1st, 2nd or 3rd degree) to the data. The SOH was calculated based on the discharge capacity of the battery. The utilized C-rate and the selection of voltage range were found to significantly affect the accuracy of the IV method. The effect of voltage range on the accuracy of the IV method for different chemistries at a charging rate of 1C is presented in Fig. 8. As can be seen from Fig. 8a, the method is particularly sensitive to selecting the correct voltage range for LFP cells. To achieve accurate results for LFP cells, the upper voltage limit should be close to the voltage corresponding to 80% SOC, and the lower voltage limit should correspond to 30% SOC or lower. For NMC cells (Fig. 8b) the accuracy of the IV method does not depend significantly on the upper voltage limit, but the lower the lower voltage limit, the better. For LTO cells (Fig. 8c) the voltage range does not appear to have a significant effect on the accuracy of the IV method, for in all voltage ranges tested the accuracy was good, although the accuracy decreased slightly in the narrowest voltage ranges.

The results of the integrated voltage method for LFP, NMC and LTO cells are presented in Fig. 9. For LFP and NMC cells, the selected voltage range corresponds to approximately 20–80% SOC, which provides accurate results for both chemistries and is still feasible in real applications. For LTO cells, the good accuracy of the method does not require as wide a voltage range, so a voltage range corresponding to approximately 40–80% SOC was selected as it is easier to implement in applications.

As can be seen from Fig. 9, the integrated voltage calculated from partial C/3, 1C and 2C charging data of the studied LFP cells has a clear correlation with the SOH of the cell (subfigures a-b). The root mean square error of the fitted models for all studied C-rates is below 2%: 1.83% with C/3, 1.67% with 1C, and 1.91% with 2C. For NMC and LTO cells (subfigures d-i) the results from C/3 charging follow the fitted model with an accuracy as high as 0.58% (RMSE) for NMC and 0.72% (RMSE) for LTO. The accuracy with 1C and 2C is slightly lower: 0.91% and 1.70%, respectively, for NMC, and 1.02% and 1.58% for LTO. Overall, the results show that the accuracy of the integrated voltage method is better with lower C-rates, but the accuracy is relatively good even with 2C charging.

Another factor affecting the accuracy of the method is the utilized voltage (or SOC) range. In this study, it was observed that a wider voltage range leads to more accurate results. From an application point of view, the narrower the required voltage range, the better. Therefore, the voltage range selected needs to be a compromise between accuracy and applicability of the method. To obtain high accuracy, relatively wide voltage range was used in this study: a voltage range corresponding to approximately 20–80% SOC for tested LFP and NMC cells, and a voltage range corresponding to approximately 40–80% SOC for tested LTO cells. Depending on the application-specific limitations, a smaller voltage range can also be used. In addition to the C-rate and voltage range, the temperature of the cell may also affect the accuracy of the IV method by changing the shape of the voltage curve during charging. The measurements in this study were performed at room temperature, so the effect of temperature remains a topic for future research.

4.2.3. Comparison of incremental capacity analysis and integrated voltage method

The accuracies of the ICA method and the IV method for different cell chemistries and C-rates are collected in Table 4. The accuracy of both the ICA and IV methods was found to depend on the magnitude of the charging current. The results for the ICA method indicate an accuracy of 0.9–2.1% (RMSE) with C/3 charging, depending on the cell chemistry. The IV method produced slightly more accurate results with C/3 charging: the accuracy of the method is 0.6–1.8% (RMSE). When the charging current was increased, the accuracy of the ICA method suffered more than that of the IV method. The results of the ICA method for the LFP cells started to scatter already with 1C, and a similar phenomenon was observed for the NMC cells with 2C. The decrease in the accuracy of the ICA method is related to the shrinkage of the characteristic IC curve peaks as the charging current is increased. The accuracy of the IV method did not suffer from increasing charging current as heavily as the accuracy of the ICA method, and the SOH estimation error remained below 2.0% (RMSE) with all studied cell types up to 2C charging.

In addition to the C-rate, another key factor influencing the accuracy and applicability of the SOH estimation methods is the required voltage range. For the ICA method the required voltage range depends on the location of the characteristic peak in the IC curve, and if the peak area is calculated, also of the width of the peak. The voltage range used in the IV method can be chosen more freely, but especially in the case of LFP cells the selected voltage range greatly affects the accuracy of the method (Section 4.2.2). In general, the IV method achieves higher accuracy than the ICA method, and the better accuracy of the IV method is emphasized if a wide voltage range is available. However, in real applications the available voltage range is often limited. If only a narrow voltage range is available, the ICA method can produce more accurate results than the IV method as long as the characteristic peak is within the voltage range. The second characteristic peak for LFP cells is located at 3.38 V (approximately 40% SOC), which is within a typical operating area, whereas accurate results for LFP cells with the IV method require rather wide voltage range (approximately 25%−80% SOC). For NMC and LTO cells the maximums of the characteristic peaks are at relatively low voltages (approximately 20–25% SOC), which places constraints on the data applicable for the ICA method. Achieving good accuracy with the IV method for NMC cells also requires relatively low voltage range

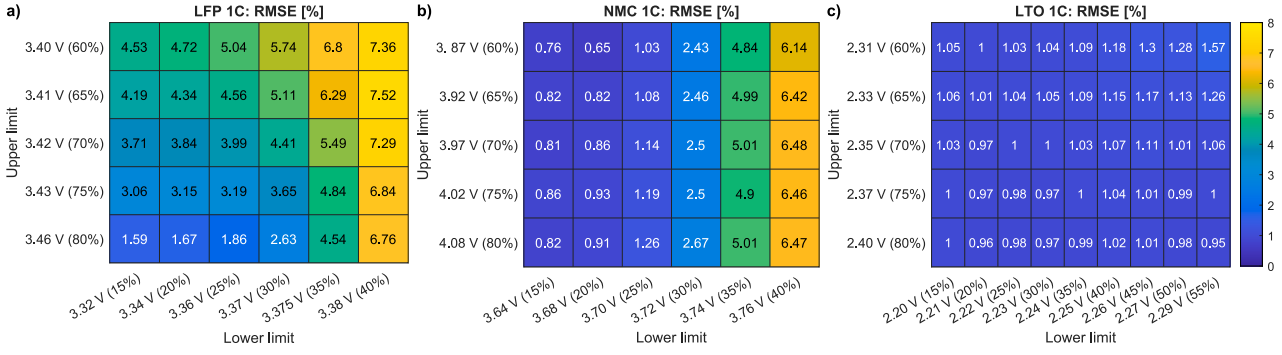

Fig. 8. The effect of voltage range on the accuracy of the IV method for LFP cells (a), NMC cells (b) and LTO cells (c). The approximate SOC corresponding to the voltage is indicated in parenthesis.

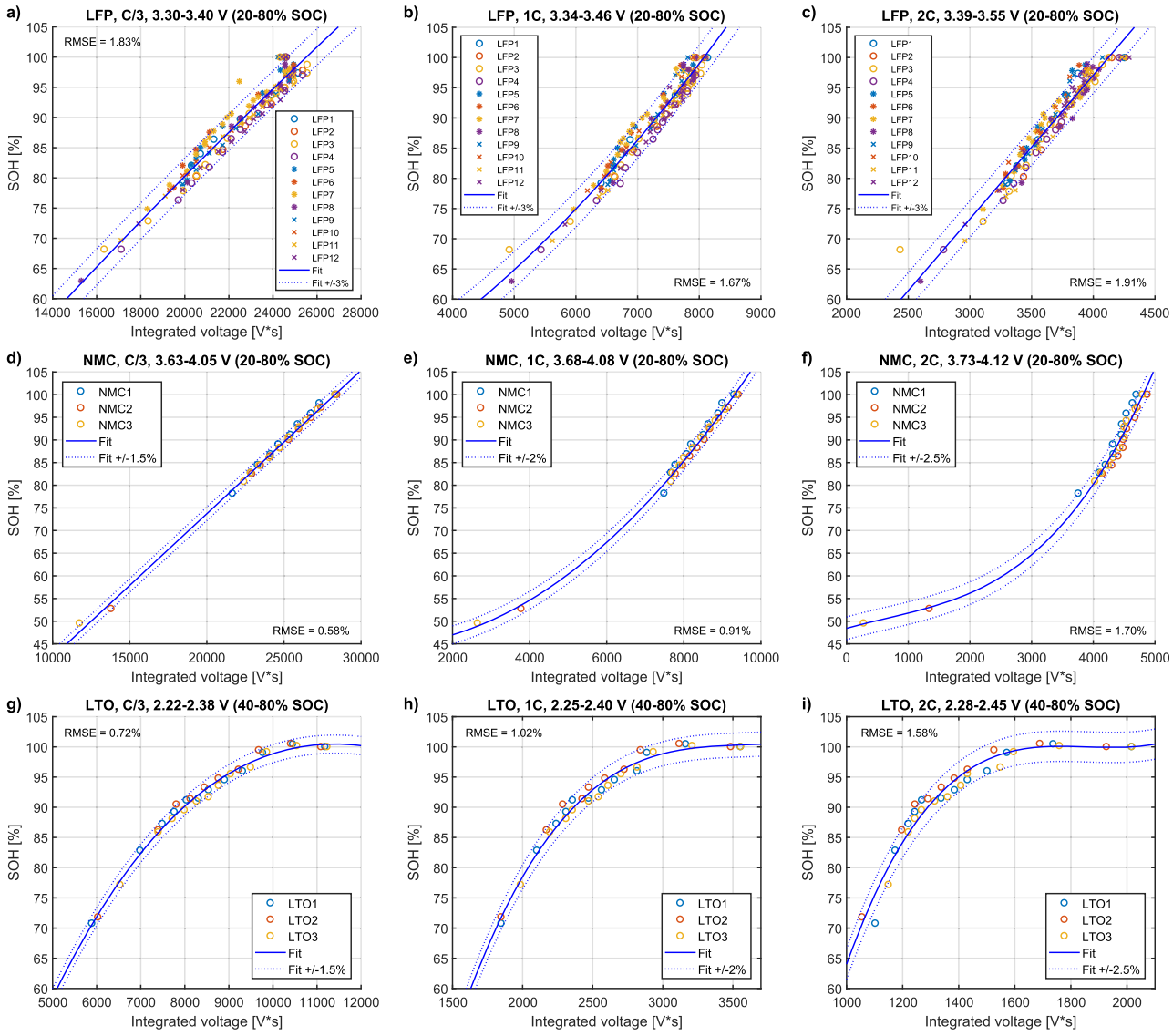

Fig. 9. The results of the integrated voltage method for LFP cells (a-c), NMC cells (d-f) and LTO cells (g-i) with different C-rates. The root mean square error (RMSE) of the fitted model is marked on each figure.

Table 4
Comparison of ICA method and IV method in terms of SOH estimation accuracy.

Cell chemistry	C-rate	ICA method RMSE	IV method RMSE
LFP	C/3	2.12%	1.83%
LFP	1C	2.33%	1.67%
LFP	2C	–	1.91%
NMC	C/3	1.37%	0.58%
NMC	1C	1.60%	0.91%
NMC	2C	4.72%	1.70%
LTO	C/3	0.85%	0.72%
LTO	1C	1.58%	1.02%
LTO	2C	1.57%	1.58%

(approximately 25–60% SOC), while for LTO cells accurate results can be obtained even with a narrow voltage range at low or high voltage (Fig. 8).

5. Conclusions

In this study, two battery SOH estimation methods were tested: incremental capacity analysis (ICA) and integrated voltage method (IV). The applicability of the methods for higher C-rates was examined utilizing partial charging data from C/3, 1C and 2C charging of commercial large format LFP, NMC and LTO cells at different stages of ageing.

The accuracy of both the ICA and IV methods was found to depend on the magnitude of the charging current. The results for the ICA method indicate an accuracy of 0.9–2.1% (RMSE) with C/3 charging, depending on the cell type. The IV method produced slightly more accurate results with C/3 charging: the accuracy of the method is 0.6–1.8% (RMSE). When the charging current was increased, the accuracy of the ICA method suffered more than that of the IV method. The results of the ICA method for the LFP cells started to scatter already with 1C, and a similar phenomenon was observed for the NMC cells with 2C. The accuracy of the IV method did not suffer from increasing charging current as heavily as the accuracy of the ICA method, and the SOH estimation error remained below 2.0% (RMSE) with all studied cell types up to 2C charging.

Another factor influencing the accuracy and applicability of the ICA and IV methods is the required voltage range. For the ICA method the required voltage range depends on the location of the characteristic peak in the IC curve. On the contrary, for the IV method the utilized voltage range can be chosen more freely, but especially in the case of LFP cells

the selected voltage range greatly affects the accuracy of the method. For NMC cells, a wide voltage range is not as important as for LFP cells, but lower voltages are required for accurate results. For LTO cells the accuracy of the IV method does not significantly depend on the utilized voltage range. In general, the IV method achieves higher accuracy than the ICA method, but if only a narrow voltage range is available, the ICA method can be more accurate than the IV method as long as the characteristic peak is within the voltage range.

The experiments for this study were performed at room temperature, and therefore the effect of temperature on the accuracy of the SOH estimation methods remains a topic for future research. As no destructive post mortem analyses were done on the cells, the same is true with insights into the actual degradation processes and their possible dependency on the C-rates and operation schemes.

The results of this study show that both the ICA method and the IV method can be used for battery SOH estimation utilizing partial charging data with relatively high C-rates. Especially the IV method has potential to be implemented on a BMS due to its simple implementation, requirement for voltage data only, and relatively good accuracy with even higher C-rates.

Funding

This work was supported by Batteries for Business (B4B) project (2017-2019), which received funding from Business Finland, and the INVADE H2020 project (2017-2019), which received funding from the European Union's Horizon 2020 Research and innovation programme under grant agreement no. 731148.

CRediT authorship contribution statement

Samppa Jenu: Methodology, Formal analysis, Writing – original draft, Writing – review & editing. **Ari Hentunen:** Writing – review & editing. **Jari Haavisto:** Investigation. **Mikko Pihlatie:** Funding acquisition, Writing – review & editing.

Declaration of Competing Interest

The authors declare no conflict of interest.

Acknowledgments

The authors thank Mr. Ville Erkkilä for his contribution to this work during the B4B project.

References

[1] A. Barré, B. Deguilhem, S. Grolleau, M. Gérard, F. Suard, D. Riu, A review on lithium-ion battery ageing mechanisms and estimations for automotive applications, J. Power Source 241 (2013) 680–689, https://doi.org/10.1016/j.jpowsour.2013.05.040.

[2] S.M. Rezvanizaniani, Z. Liu, Y. Chen, J. Lee, Review and recent advances in battery health monitoring and prognostics technologies for electric vehicle (EV) safety and mobility, J. Power Source 256 (2014) 110–124, https://doi.org/10.1016/j.jpowsour.2014.01.085.

[3] J. Vetter, P. Novák, M.R. Wagner, C. Veit, K.C. Möller, J.O. Besenhard, M. Winter, M. Wohlfahrt-Mehrens, C. Vogler, A. Hammouche, Ageing mechanisms in lithium-ion batteries, J. Power Source 147 (2005) 269–281, https://doi.org/10.1016/j.jpowsour.2005.01.006.

[4] C.R. Birkl, M.R. Roberts, E. Mcturk, P.G. Bruce, D.A. Howey, Degradation diagnostics for lithium ion cells, J. Power Source 341 (2017) 373–386, https://doi.org/10.1016/j.jpowsour.2016.12.011.

[5] J. Wang, P. Liu, J. Hicks-Garner, E. Sherman, S. Soukiazian, M. Verbrugge, H. Tataria, J. Musser, P. Finamore, Cycle-life model for graphite-LiFePO4 cells, J. Power Source 196 (2011) 3942–3948, https://doi.org/10.1016/j.jpowsour.2010.11.134.

[6] N. Omar, M.A. Monem, Y. Firouz, J. Salminen, J. Smekens, O. Hegazy, H. Gaulous, G. Mulder, P. Van den Bossche, T. Coosemans, J. Van Mierlo, Lithium iron phosphate based battery - Assessment of the aging parameters and development of cycle life model, Appl. Energy 113 (2014) 1575–1585, https://doi.org/10.1016/j.apenergy.2013.09.003.

[7] L. Lam, P. Bauer, Practical capacity fading model for Li-ion battery cells in electric vehicles, IEEE Trans. Power Electron. 28 (2013) 5910–5918, https://doi.org/10.1109/TPEL.2012.2235083.

[8] J. Groot, M. Swierczynski, A.I. Stan, S.K. Kær, On the complex ageing characteristics of high-power LiFePO<inf>4</inf>/graphite battery cells cycled with high charge and discharge currents, J. Power Source 286 (2015) 475–487, https://doi.org/10.1016/j.jpowsour.2015.04.001.

[9] M. Naumann, F. Spingler, A. Jossen, Analysis and modeling of cycle aging of a commercial LiFePO4/graphite cell, J. Power Source 451 (2020), 227666, https://doi.org/10.1016/j.jpowsour.2019.227666.

[10] M. Schimpe, M.E. von Kuepach, M. Naumann, H.C. Hesse, K. Smith, A. Jossen, Comprehensive modeling of temperature-dependent degradation mechanisms in lithium iron phosphate batteries, J. Electrochem. Soc. 165 (2018) A181–A193, https://doi.org/10.1149/2.1181714jes.

[11] J. Jiang, W. Shi, J. Zheng, P. Zuo, J. Xiao, X. Chen, W. Xu, J.-.G. Zhang, Optimized operating range for large-format LiFePO4/graphite batteries, J. Electrochem. Soc. 161 (2013) A336–A341, https://doi.org/10.1149/2.052403jes.

[12] M. Lewerenz, J. Münnix, J. Schmalstieg, S. Käbitz, M. Knips, D.U. Sauer, Systematic aging of commercial LiFePO4|Graphite cylindrical cells including a theory explaining rise of capacity during aging, J. Power Source 345 (2017) 254–263, https://doi.org/10.1016/j.jpowsour.2017.01.133.

[13] M. Ecker, N. Nieto, S. Käbitz, J. Schmalstieg, H. Blanke, A. Warnecke, D.U. Sauer, Calendar and cycle life study of Li(NiMnCo)O2-based 18650 lithium-ion batteries, J. Power Source 248 (2014) 839–851, https://doi.org/10.1016/j.jpowsour.2013.09.143.

[14] S.F. Schuster, T. Bach, E. Fleder, J. Müller, M. Brand, G. Sextl, A. Jossen, Nonlinear aging characteristics of lithium-ion cells under different operational conditions, J. Energy Storage. 1 (2015) 44–53, https://doi.org/10.1016/j.est.2015.05.003.

[15] D. Li, H. Li, D.L. Danilov, L. Gao, X. Chen, Z. Zhang, J. Zhou, R.A. Eichel, Y. Yang, P.H.L. Notten, Degradation mechanisms of C6/LiNi0.5Mn0.3Co0.2O2 Li-ion batteries unraveled by non-destructive and post-mortem methods, J. Power Source 416 (2019) 163–174, https://doi.org/10.1016/j.jpowsour.2019.01.083.

[16] A. Maheshwari, M. Heck, M. Santarelli, Cycle aging studies of lithium nickel manganese cobalt oxide-based batteries using electrochemical impedance spectroscopy, Electrochim. Acta 273 (2018) 335–348, https://doi.org/10.1016/j.electacta.2018.04.045.

[17] S. Käbitz, J.B. Gerschler, M. Ecker, Y. Yurdagel, B. Emmermacher, D. André, T. Mitsch, D.U. Sauer, Cycle and calendar life study of a graphite|LiNi1/3Mn 1/3Co1/3O2 Li-ion high energy system. Part A: full cell characterization, J. Power Source 239 (2013) 572–583, https://doi.org/10.1016/j.jpowsour.2013.03.045.

[18] K. Jalkanen, J. Karppinen, L. Skogström, T. Laurila, M. Nisula, K. Vuorilehto, Cycle aging of commercial NMC/graphite pouch cells at different temperatures, Appl. Energy 154 (2015) 160–172, https://doi.org/10.1016/j.apenergy.2015.04.110.

[19] F. Richter, P.J.S. Vie, S. Kjelstrup, O.S. Burheim, Measurements of ageing and thermal conductivity in a secondary NMC-hard carbon Li-ion battery and the impact on internal temperature profiles, Electrochim. Acta 250 (2017) 228–237, https://doi.org/10.1016/j.electacta.2017.07.173.

[20] J. de Hoog, J.M. Timmermans, D. Ioan-Stroe, M. Swierczynski, J. Jaguemont, S. Goutam, N. Omar, J. Van Mierlo, P. Van Den Bossche, Combined cycling and calendar capacity fade modeling of a Nickel-Manganese-Cobalt Oxide Cell with real-life profile validation, Appl. Energy 200 (2017) 47–61, https://doi.org/10.1016/j.apenergy.2017.05.018.

[21] J.M. Reniers, G. Mulder, S. Ober-Blöbaum, D.A. Howey, Improving optimal control of grid-connected lithium-ion batteries through more accurate battery and degradation modelling, J. Power Source 379 (2018) 91–102, https://doi.org/10.1016/j.jpowsour.2018.01.004.

[22] Y. Gao, J. Jiang, C. Zhang, W. Zhang, Y. Jiang, Aging mechanisms under different state-of-charge ranges and the multi-indicators system of state-of-health for lithium-ion battery with Li(NiMnCo)O2 cathode, J. Power Source 400 (2018) 641–651, https://doi.org/10.1016/j.jpowsour.2018.07.018.

[23] M. Lewerenz, D.U. Sauer, Evaluation of cyclic aging tests of prismatic automotive LiNiMnCoO2-graphite cells considering influence of homogeneity and anode overhang, J. Energy Storage. 18 (2018) 421–434, https://doi.org/10.1016/j.est.2018.06.003.

[24] M. Lucu, E. Martinez-Laserna, I. Gandiaga, K. Liu, H. Camblong, W.D. Widanage, J. Marco, Data-driven nonparametric Li-ion battery ageing model aiming at learning from real operation data - Part B: cycling operation, J. Energy Storage. 30 (2020), 101410, https://doi.org/10.1016/j.est.2020.101410.

[25] N. Takami, H. Inagaki, Y. Tatebayashi, H. Saruwatari, K. Honda, S. Egusa, High-power and long-life lithium-ion batteries using lithium titanium oxide anode for automotive and stationary power applications, J. Power Source 244 (2013) 469–475, https://doi.org/10.1016/j.jpowsour.2012.11.055.

[26] X. Han, M. Ouyang, L. Lu, J. Li, Cycle life of commercial lithium-ion batteries with lithium titanium oxide anodes in electric vehicles, Energies 7 (2014) 4895–4909, https://doi.org/10.3390/en7084895.

[27] A.I. Stroe, D.L. Stroe, V. Knap, M. Swierczynski, R. Teodorescu, Accelerated lifetime testing of high power lithium titanate oxide batteries, in: 2018 IEEE Energy Convers. Congr. Expo. ECCE 2018., 2018, pp. 3857–3863, https://doi.org/10.1109/ECCE.2018.8557416.

[28] M. Dubarry, A. Devie, Battery durability and reliability under electric utility grid operations: representative usage aging and calendar aging, J. Energy Storage. 18 (2018) 185–195, https://doi.org/10.1016/j.est.2018.04.004.

[29] S. Liu, M. Winter, M. Lewerenz, J. Becker, D.U. Sauer, Z. Ma, J. Jiang, Analysis of cyclic aging performance of commercial Li4Ti5O12-based batteries at room temperature, Energy 173 (2019) 1041–1053, https://doi.org/10.1016/j.energy.2019.02.150.

[30] R. Xiong, L. Li, J. Tian, Towards a smarter battery management system: a critical review on battery state of health monitoring methods, J. Power Source 405 (2018) 18–29, https://doi.org/10.1016/j.jpowsour.2018.10.019.
[31] M. Berecibar, I. Gandiaga, I. Villarreal, N. Omar, J. Van Mierlo, P. Van Den Bossche, Critical review of state of health estimation methods of Li-ion batteries for real applications, Renew. Sustain. Energy Rev. 56 (2016) 572–587, https://doi.org/10.1016/j.rser.2015.11.042.
[32] L. Ungurean, G. Cârstoiu, M.V. Micea, V. Groza, Battery state of health estimation: a structured review of models, methods and commercial devices, Int. J. Energy Res. 41 (2017) 151–181, https://doi.org/10.1002/er.3598.
[33] M.S.H. Lipu, M.A. Hannan, A. Hussain, M.M. Hoque, P.J. Ker, M.H.M. Saad, A. Ayob, A review of state of health and remaining useful life estimation methods for lithium-ion battery in electric vehicles: challenges and recommendations, J. Clean. Prod. (2018), https://doi.org/10.1016/j.jclepro.2018.09.065.
[34] K.S. Ng, C.S. Moo, Y.P. Chen, Y.C. Hsieh, Enhanced coulomb counting method for estimating state-of-charge and state-of-health of lithium-ion batteries, Appl. Energy. 86 (2009) 1506–1511, https://doi.org/10.1016/j.apenergy.2008.11.021.
[35] Y. Bao, W. Dong, D. Wang, Online internal resistance measurement application in lithium ion battery capacity and state of charge estimation, Energies (2018) 11, https://doi.org/10.3390/en11051073.
[36] C. Pastor-Fernández, K. Uddin, G.H. Chouchelamane, W.D. Widanage, J. Marco, A comparison between electrochemical impedance spectroscopy and incremental capacity-differential voltage as Li-ion diagnostic techniques to identify and quantify the effects of degradation modes within battery management systems, J. Power Source 360 (2017) 301–318, https://doi.org/10.1016/j.jpowsour.2017.03.042.
[37] M. Dubarry, B.Y. Liaw, M.S. Chen, S.S. Chyan, K.C. Han, W.T. Sie, S.H. Wu, Identifying battery aging mechanisms in large format Li ion cells, J. Power Source 196 (2011) 3420–3425, https://doi.org/10.1016/j.jpowsour.2010.07.029.
[38] X. Han, M. Ouyang, L. Lu, J. Li, A comparative study of commercial lithium ion battery cycle life in electric vehicle: capacity loss estimation, J. Power Source 268 (2014) 658–669, https://doi.org/10.1016/j.jpowsour.2014.06.111.
[39] E. Riviere, P. Venet, A. Sari, F. Meniere, Y. Bultel, LiFePO4 battery state of health online estimation using electric vehicle embedded incremental capacity analysis, in: 2015 IEEE Veh. Power Propuls. Conf. VPPC 2015 - Proc, 2015, https://doi.org/10.1109/VPPC.2015.7352972.
[40] M. Berecibar, F. Devriendt, M. Dubarry, I. Villarreal, N. Omar, W. Verbeke, J. Van Mierlo, Online state of health estimation on NMC cells based on predictive analytics, J. Power Source 320 (2016) 239–250, https://doi.org/10.1016/j.jpowsour.2016.04.109.
[41] C. Weng, X. Feng, J. Sun, H. Peng, State-of-health monitoring of lithium-ion battery modules and packs via incremental capacity peak tracking, Appl. Energy 180 (2016) 360–368, https://doi.org/10.1016/j.apenergy.2016.07.126.
[42] Y. Li, M. Abdel-Monema, R. Gopalakrishnan, M. Berecibar, E. Nanini-Maury, N. Omar, P. van den Bossche, J. Van Mierlo, A quick on-line state of health estimation method for Li-ion battery with incremental capacity curves processed by Gaussian filter, J. Power Source 373 (2018) 40–53, https://doi.org/10.1016/j.jpowsour.2017.10.092.
[43] X. Tang, C. Zou, K. Yao, G. Chen, B. Liu, Z. He, F. Gao, A fast estimation algorithm for lithium-ion battery state of health, J. Power Source 396 (2018) 453–458, https://doi.org/10.1016/j.jpowsour.2018.06.036.
[44] Y. Jiang, J. Jiang, C. Zhang, W. Zhang, Y. Gao, N. Li, State of health estimation of second-life LiFePO 4 batteries for energy storage applications, J. Clean. Prod. (2018), https://doi.org/10.1016/j.jclepro.2018.09.149.
[45] D. Ansean, V.M. Garcia, M. Gonzalez, C. Blanco-Viejo, J.C. Viera, Y.F. Pulido, L. Sanchez, Lithium-ion battery degradation indicators via incremental capacity analysis, IEEE Trans. Ind. Appl. 55 (2019) 2992–3002, https://doi.org/10.1109/TIA.2019.2891213.
[46] E. Riviere, A. Sari, P. Venet, F. Meniere, Y. Bultel, Innovative incremental capacity analysis implementation for c/lifepo 4 cell state-of-health estimation in electrical vehicles, Batteries 5 (2019), https://doi.org/10.3390/batteries5020037.
[47] N. Wassiliadis, J. Adermann, A. Frericks, M. Pak, C. Reiter, B. Lohmann, M. Lienkamp, Revisiting the dual extended Kalman filter for battery state-of-charge and state-of-health estimation: a use-case life cycle analysis, J. Energy Storage. 19 (2018) 73–87, https://doi.org/10.1016/j.est.2018.07.006.
[48] D.I. Stroe, V. Knap, E. Schaltz, State-of-health estimation of lithium-ion batteries based on partial charging voltage profiles, ECS Trans. 85 (2018) 379–386, https://doi.org/10.1149/08513.0379ecst.
[49] E. Schaltz, D.I. Stroe, K. Norregaard, B. Johnsen, A. Christensen, Partial charging method for lithium-ion battery state-of-health estimation, in: 2019 14th Int. Conf. Ecol. Veh. Renew. Energies, EVER 2019, 2019, pp. 4–8, https://doi.org/10.1109/EVER.2019.8813645.
[50] Y. Zhou, M. Huang, M. Pecht, An online state of health estimation method for lithium-ion batteries based on integrated voltage, in: 2018 IEEE Int. Conf. Progn. Heal. Manag. ICPHM 2018., 2018, https://doi.org/10.1109/ICPHM.2018.8448947.